

Constraining the photon coupling of ultra-light dark-matter axion-like particles by polarization variations of parsec-scale jets in active galaxies

M.M. Ivanov,^{a,b,c} Y.Y. Kovalev,^{d,e} M.L. Lister,^f A.G. Panin,^{a,e}
A.B. Pushkarev,^{g,d} T. Savolainen,^{h,i} and S.V. Troitsky^{a,1}

^aInstitute for Nuclear Research of the Russian Academy of Sciences, 60th October Anniversary Prospect 7a, Moscow 117312, Russia

^bSchool of Natural Sciences, Institute for Advanced Study, 1 Einstein Drive, Princeton, NJ 08540, USA

^cInstitute of Physics, Laboratory of Particle Physics and Cosmology (LPPC), École Polytechnique Fédérale de Lausanne, CH-1015, Lausanne, Switzerland

^dAstro Space Center, P. N. Lebedev Physical Institute, Russian Academy of Sciences, Profsoyuznaya 84/32, Moscow, 117997, Russia

^eMoscow Institute of Physics and Technology, Institutsky per. 9, Dolgoprudny, 141700, Russia

^fDepartment of Physics and Astronomy, Purdue University, 525 Northwestern Avenue, West Lafayette, IN 47907, USA

^gCrimean Astrophysical Observatory, Russian Academy of Sciences, Nauchny, 298409, Russia

^hAalto University Department of Electronics and Nanoengineering, PL 15500, 00076 Aalto, Finland

ⁱAalto University Metsähovi Radio Observatory, Metsähovintie 114, 02540 Kylmälä, Finland

E-mail: st@ms2.inr.ac.ru

Abstract. Ultra-light dark matter may consist of axion-like particles with masses below 10^{-19} eV. Two-photon interactions of these particles affect the polarization of radiation propagating through the dark matter. Coherent oscillations of the Bose condensate of the particles induce periodic changes in the plane of polarisation of emission passing through the condensate. We estimate this effect and analyze MOJAVE VLBA polarization observations of bright downstream features in the parsec-scale jets of active galaxies. Through the non-observation of periodic polarization changes, we are able to constrain the photon coupling of the ultra-light dark-matter axion-like particles at the level of $\lesssim 10^{-12}$ GeV⁻¹ for masses between $\sim 5 \times 10^{-23}$ eV and $\sim 1.2 \times 10^{-21}$ eV.

¹Corresponding author.

Contents

1	Introduction	1
2	Theoretical calculation of the expected effect	2
3	The data	4
4	The analysis method	6
5	Results and discussion	9
6	Conclusions	12
A	Generalized Lomb–Scargle periodogram	14
B	Monte-Carlo simulations and expected limits	15
	B.1 Monte-Carlo simulation	15
	B.2 Estimate of the expected limits	15

1 Introduction

Despite impressive experimental efforts towards direct-detection, collider and indirect searches for weakly interacting massive particles (WIMPs, see e.g. Refs. [1–3] for corresponding reviews), no confirmation of the existence of a candidate dark-matter (DM) particle of this kind has been obtained. As a result, we witness a growing interest to non-WIMP DM candidates, including axions, axion-like particles, sterile neutrinos etc. On the other hand, the conventional Cold Dark Matter (CDM) scenario suffers from considerable tensions with observational data regarding structure formation at small (below kiloparsec) scales, see e.g. Ref. [4] for a review. These tensions include the “missing satellites” [5, 6], “too-big-to-fail” [7] and “cusp-core” [8] problems. In general, CDM, as a cold, scale-free and non-interacting substance, forms too much structure at small scales.

One of the scenarios put forward to overcome these tensions is based on the concept of ultra-light (UL), also called “fuzzy”, dark matter (see e.g. Refs. [9–11], but also early pioneering works [12–14] and, for reviews, [15, 16]). In this approach, the DM particle is so light that its de Broglie wavelength is of the order of a kiloparsec, the “problematic” scale of structure formation. This corresponds to a DM particle mass of order of $m \sim 10^{-22}$ eV. With this low mass, the observed DM energy density requires very high number densities of the ULDM particles, which imply that they exist in the form of a classical bosonic field, or a Bose condensate. To protect the low mass from radiative corrections, it is often assumed that the ULDM field corresponds to a pseudo-Goldstone boson of some broken symmetry, just like the Quantum Chromodynamics (QCD) axion is related to breaking of the Peccei-Quinn symmetry. Related to QCD or not, this particle develops a non-renormalizable coupling to photons similar to that of the axion. Pseudoscalars with these couplings are called axion-like particles (ALPs, see e.g. Ref. [17] for a review). They appear in a natural way in many extensions of the Standard Model of particle physics, including those related to string theory [18–20].

The photon coupling of ALPs makes it possible to search for their manifestations in laboratory experiments and in astrophysical environments, see e.g. Refs. [15, 21–23] for recent reviews. A range of approaches are based on the ALP-photon mixing in external magnetic fields [24], which results in the ALP-photon oscillations, the ALP Primakoff effect and vacuum birefringence. Here, we follow a different approach which is based on the same ALP-photon interaction: the polarization properties of light are changed when it propagates in the external pseudoscalar field.

The condensate of ULDM particles is naturally produced in the early Universe, as follows both from analytical estimates and from detailed numerical simulations. The produced condensate forms domains of the size of order ~ 100 pc (see e.g. Ref. [25] for a numerical demonstration). Within each clump, the ALP field experiences fast coherent oscillations with the period determined by m . These oscillations can be used to constrain the ULDM scenario with pulsar timing arrays [26–28]. In the present work, we explore the effect of these coherent oscillations on the propagation of electromagnetic waves through the ULDM condensate. We demonstrate that the polarization angle of linearly polarized emission oscillates with the same period, which is determined by the ALP mass and is therefore uniform for all ALP domains in the Universe. Then, we use long-term observations of polarization properties of radio sources to search for these oscillations. We do not find any significant evidence for oscillations with a common period and use this fact to constrain the photon coupling of the ULDM ALP.

The rest of the paper is organized as follows. In Section 2, we consider photon propagation in the oscillating external ALP background and demonstrate that the plane of linear polarization of photons oscillates with the same period. In Section 3, we describe the data resulted from long-term radio observations of parsec-scale jets in active galaxies which we use in this paper. Section 4 presents the method to search, in the ensemble of data, for oscillations with a common period but arbitrary phase. In Section 5, we present our results and derive constraints on the ALP-photon coupling. We briefly conclude in Section 6, while some technical details are presented in Appendices.

2 Theoretical calculation of the expected effect

We start with the following Lagrangian for an ALP interacting with photons,

$$\mathcal{L} = -\frac{1}{4}F_{\mu\nu}^2 + \frac{1}{2}(\partial_\mu a \partial^\mu a - m^2 a^2) + \frac{g_{a\gamma}}{4} a F_{\mu\nu} \tilde{F}^{\mu\nu},$$

where a is the ALP field, $F_{\mu\nu}$ is the electromagnetic stress tensor, $\tilde{F}^{\mu\nu} = \frac{1}{2}\epsilon^{\mu\nu\rho\sigma}F^{\rho\sigma}$ and ALP parameters are the mass m and the photon coupling constant $g_{a\gamma}$. The latter has the dimension of inverse mass in the natural ($\hbar = c = 1$) system of units, which we hereafter use, unless the dimensions are written explicitly. The Minkowski sum over repeating Greek indices $\mu, \nu, \lambda, \rho = 0, \dots, 3$ is assumed (Latin indices $i, j = 1, 2, 3$ enumerate the spatial coordinates).

The equations of motion for the electromagnetic field read

$$\partial_\mu F^{\mu\nu} + \frac{1}{2}g_{a\gamma}\epsilon^{\mu\nu\lambda\rho}\partial_\mu(aF_{\lambda\rho}) = 0.$$

At the scales of order the photon wavelength, a changes slowly and hence can be treated adiabatically when taking Fourier integrals. To study the effect of the external a field on the polarization, we consider a plane-wave Ansatz for the electromagnetic field,

$$A_\nu(x) = A_\nu(k)e^{ikx} + \text{h. c.},$$

and decompose $A_\nu(k)$ into two linearly polarized components,

$$A_\nu = A^+ e_\nu^+ + A^- e_\nu^-,$$

where e_ν^\pm are properly chosen polarization vectors. The equations of motion result in the dispersion relations (we use here the fact that $|\partial_0 a| \sim m|a|$ while $|\partial_i a| \sim mv|a|$, where $v \ll 1$ is the dark-matter velocity, hence $|\partial_0 a| \ll |\partial_i a|$),

$$\omega_\pm^2 - k^2 \mp g_{a\gamma} \partial_0 a |k| = 0,$$

so the two polarization states propagate with

$$\omega_\pm = k \sqrt{1 \pm g_{a\gamma} \frac{\partial_0 a}{k}} \simeq k \pm \frac{1}{2} g_{a\gamma} \partial_0 a$$

(see also Refs. [19, 29]).

The axion condensate acts as an optically active medium, in which a linearly polarized photon acquires a phase shift between two circular polarizations, which results in the rotation of the polarization plane. This effect as a *cosmological birefringence* has been constrained in the past, see e.g. [30–33]. Recent studies [34–36] suggested to test this effect with laser interferometry. It should be noted that these works were considering a constant phase shift experienced by photons. In contrast, in the present work we focus on the *periodic* changes of the phase shift caused by the oscillating ALP background.

The difference between the frequencies of the two polarization components,

$$\Delta\omega = g_{a\gamma} \partial_0 a,$$

is translated into the change of the polarization angle for a linearly polarized emission,

$$\Delta\phi = \frac{1}{2} \int_{t_1}^{t_2} \Delta\omega dt = \frac{1}{2} g_{a\gamma} \int_{t_1}^{t_2} \partial_0 a dt,$$

where the integration is performed along the propagation path of the electromagnetic wave from the emission moment t_1 to the observation moment t_2 . We use again $|\partial_0 a| \ll |\partial_i a|$ to write

$$\partial_0 a \equiv \frac{da}{dt} - \frac{k_i}{|k|} \partial_i a \simeq \frac{da}{dt}$$

and therefore obtain

$$\Delta\phi = \frac{1}{2} g_{a\gamma} (a(t_2) - a(t_1)).$$

Note that the effect is frequency-independent and depends only on the local value of the ALP field at the source and the observer. This is true even in the case of inhomogeneous background [29].

The ALP field is coherent and homogeneous at the scales of order of

$$\lambda = \frac{1}{mv} \simeq 65 \left(\frac{m}{10^{-22} \text{ eV}} \right)^{-1} \left(\frac{v}{10^{-3}} \right)^{-1} \text{ pc},$$

where v is the mean velocity of dark matter. It oscillates as

$$a(t) = a_0 \sin(mt + \delta),$$

where δ is some random phase and a_0 is the field amplitude. The typical oscillation period is

$$T = \frac{2\pi}{m} \simeq 4 \cdot 10^7 \left(\frac{10^{-22} \text{ eV}}{m} \right) \text{ sec.} \quad (2.1)$$

Therefore, these background oscillations get imprinted in the oscillations of the photon phase shift. The observed period at the Earth is $T' = T(1+z)$, where z is the redshift of the source.

We will be interested in the situation where the ALP field in the vicinity of the source is much stronger than next to the observer, that is $a(t_2) \ll a(t_1)$. In particular, this is true for central parts of elliptical galaxies hosting AGNs, which have a reasonably high dark-matter density. Indeed, a recent joint analysis of lensing and kinematics data from Ref. [37] gives the following estimate for the dark-matter energy density there,

$$\rho_{\text{DM}} \sim 5 \cdot 10^9 M_{\odot}/\text{kpc}^3 \simeq 20 \text{ GeV}/\text{cm}^3.$$

Here we assumed a typical dark-matter fraction in elliptical galaxies $\sim 50\%$ [38]. On the other hand, the energy density

$$\rho_{\text{DM}} = \frac{1}{2} \langle (\partial a)^2 \rangle + \frac{m^2}{2} \langle a^2 \rangle = \frac{1}{2} m^2 a_0^2,$$

which we use to express a_0 through ρ_{DM} and to obtain the final expression for the oscillating shift of the polarization angle,

$$\Delta\phi \simeq 5^\circ \sin \left(2\pi \frac{t}{T'} + \delta \right) \left(\frac{\rho_{\text{DM}}}{20 \text{ GeV}/\text{cm}^3} \right)^{\frac{1}{2}} \left(\frac{g_{a\gamma}}{10^{-12} \text{ GeV}^{-1}} \right) \left(\frac{m}{10^{-22} \text{ eV}} \right)^{-1}. \quad (2.2)$$

3 The data

For the purposes of our study, we made use of polarization sensitive interferometric data at 15 GHz primarily from the MOJAVE (Monitoring Of Jets in Active galactic nuclei with VLBA Experiments) program to monitor radio brightness and polarization variations in jets associated with active galaxies with declinations above -30° , with supplementary data obtained from the NRAO archive. The observations were performed between 1997 April 6 and 2017 August 25 with the VLBA (Very Long Baseline Array), a system of ten 25-meter radio telescopes, allowing to probe highly-collimated relativistic outflows of the observed sources on parsec scales by achieving angular resolution of the order of one milliarcsecond. The fully-calibrated visibility data together with reconstructed FITS images are publicly available online from the MOJAVE web site¹. An example of a total intensity and linear polarization image for the active galaxy 3C 120 is shown in Figure 1. The data reduction, including initial calibration and editing, was performed with the NRAO Astronomical Image Processing System [39] using the standard techniques. Imaging was done with the Caltech DIFMAP package [40]. Each of the final single-epoch images was constructed by applying natural weighting to the visibility function and a pixel size of 0.1 mas. A more detailed discussion of the data reduction and imaging process schemes can be found in [41, 46]. The earlier papers of the MOJAVE program have focused on the parsec-scale kinematics of the jets [42], their acceleration and collimation [43], circular and linear polarization properties [44–48].

¹<http://www.physics.purdue.edu/astro/MOJAVE/allsources.html>

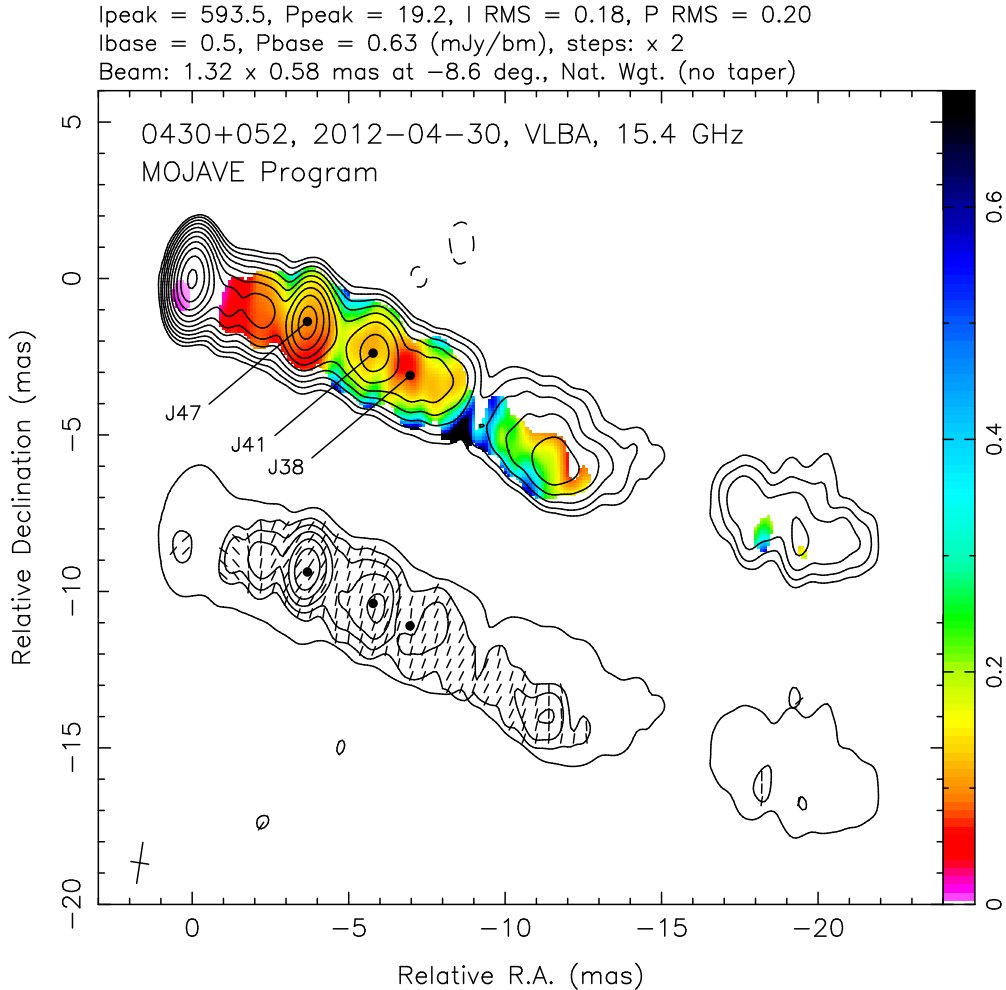


Figure 1. Parsec-scale image of the jet in the active galaxy 3C 120 observed by the Very Long Baseline Array at 2 cm within the MOJAVE program. Top: total intensity contour plot overlaid by the fractional polarization distribution represented by the color. Bottom: the lowest contour of the total intensity distribution showing the shape of the jet overlaid by the contour plot of the linear polarization map. The sticks represent the electric vector position angle (EVPA). Black bullets show the positions of the jet components used in our analysis, with labels according to their IDs in Table 1. The synthesized VLBA beam is shown at the half-power level in the bottom left corner.

To analyze the polarization evolution in the observed sources, the following approach is used. The structure of every source in its full intensity is modelled using the Caltech DIFMAP package [40] by fitting a series of circular (rarely elliptical) Gaussian components to the calibrated visibility data. These components are cross-identified at a certain number of epochs, while they remain sufficiently bright. Their electric vector position angles, $EVPA = (1/2)\arctan(U/Q)$, where U and Q are Stokes parameters, are calculated from the corresponding polarization maps as the nine-pixel average of the area centered over a position of the component in total intensity. In this way, jet and core components are identified in Refs. [42, 49]. Because of variable optical depth [50], Faraday depth and higher turbulence [51], the core components demonstrate, on average, larger EVPA fluctuations [47]. In this work, we therefore concentrate only on the jet features. We estimate that our VLBA EVPA

measurements are accurate within $\sim 5^\circ$, as it comes from a comparison of highly-compact AGNs to near-simultaneous single-dish observations.

The uncertainty in the EVPA measurements is dominated by two factors, see e.g. the Appendix of Ref. [52]. The first one is the imperfectness of the receivers which results in the effect of the instrumental polarization when the signal flows from one branch to another. The second one is related to the non-uniform coverage of the uv plane. The flow of the polarized signal is proportional to the total intensity and is therefore non-uniformly distributed over the map. It also results in an artificial increase of the signal-to-noise ratio, so that for weak signals one needs to introduce additional corrections for non-Gaussian distribution of errors. This motivates the removal of low-intensity sources from the data set to suppress hard to control instrumental errors. We impose a cut of the minimal polarized flux density of the component (the sum of polarised emission under the area of a given Gaussian component, as defined above) of 5 mJy, which guarantees that the estimated uncertainty in every particular EVPA measurement is $\sim 5^\circ$.

To perform a reliable search for periodicity at the scales of ~ 1 yr, as it would be expected for the ULDM effect, we select the source components for which the 5 mJy condition was satisfied for at least 10 observational epochs and require the cadence of not less than 5 epochs per year. Among all observations, these criteria are satisfied for one or more components of 10 sources listed in Table 1, which are used in this analysis.

The separations between jet components in a source are sufficiently large to make the regions causally disconnected at the period of observations, therefore making correlated periodic changes of the intrinsic polarization impossible. Other systematic effects could result in common EVPA variations among components of a given extragalactic radio source. First of all, it is the EVPA absolute calibration error. This error is the same for all core and jet components of all sources observed within the same 24-hour long MOJAVE VLBA epoch. Typically, 20 to 30 targets are observed. The variable fraction of this error is estimated to be less than 2° . Second, polarized emission might partly “leak” from one component to another if they are located too close to each other — within one VLBA beam. Such a situation happens not more than in a couple of cases in our sample. Finally, let us consider Faraday rotation around an extragalactic jet or in our Galaxy. Causality arguments prevent synchronous Faraday depth changes around jets since components are located far enough from each other, while the Galactic Faraday rotation is low and varies on timescales significantly longer than what is analyzed in this paper, see e.g. [53, 54]. We conclude that the common EVPA variations of components within a given target are insignificant and cannot influence results of our analysis. We note that the analysis presented in this paper was repeated for a subsample which has only one component per target. We obtained qualitatively similar results but with weaker upper limits, as it is expected from the reduction in statistics.

4 The analysis method

The aim of the present study is to search for, or to constrain, periodic oscillations of EVPA in different sources but with a common period. The data analysis we perform includes processing time-dependent measurements for every particular source in the sample to reveal indications for periodicity, followed by an analysis of the sample to see if the periodicities have one common period. We need a quantitative measure of the strength of the effect, which is compared to the same quantity obtained from the Monte-Carlo simulated data assuming no effect is present.

B1950 name	Other ID	Redshift	Component ID	Time coverage, years	Number of epochs
0415+379	3C 111	0.0491	40	4.80	40
			39	3.49	19
			30	1.94	19
			35	1.23	13
			36	1.47	19
			37	2.01	13
			39	3.49	19
			57	1.42	11
0430+052	3C 120	0.033	41	1.80	10
			38	1.23	11
			47	0.92	11
0851+202	OJ 287	0.306	22	3.15	16
			9	1.41	10
1226+023	3C 273	0.1583	19	2.49	13
			24	1.60	13
			25	1.60	12
1253−055	3C 279	0.536	6	2.97	17
1308+326	OP 313	0.997	5	2.57	13
1510−089	PKS 1510−08	0.36	15	1.65	14
			19	1.30	13
1641+399	3C 345	0.593	11	2.35	13
2200+420	BL Lac	0.0686	7	20.39	126
			20	5.09	45
			23	5.58	59
			24	2.81	25
			25	2.55	21
			26	1.70	20
			27	1.64	25
			36	0.66	11
2251+158	3C 454.3	0.859	13	1.98	10
			8	1.92	10

Table 1. List of source components selected for the analysis. MOJAVE ID and Component ID correspond to the MOJAVE catalog [42, 49]. Components with the longest time coverage are indicated in bold.

For every sequence of the EVPA measurements (a source component), we calculate the generalised Lomb-Scargle periodogram [55] (see Refs. [56, 57] for detailed discussions). Compared to other methods, it is more suitable for the case when measurements are distributed non-uniformly in time. It also accounts correctly for a non-zero mean of the measurements. For convenience, the calculation of the periodogram is summarized in Appendix A. As a result, we obtain p -values as a function of the assumed oscillation period T (rescaled from the observed T' by $(1+z)$, see Sec.2). We consider periods between 0.1 yr and 1.5 yr with a step

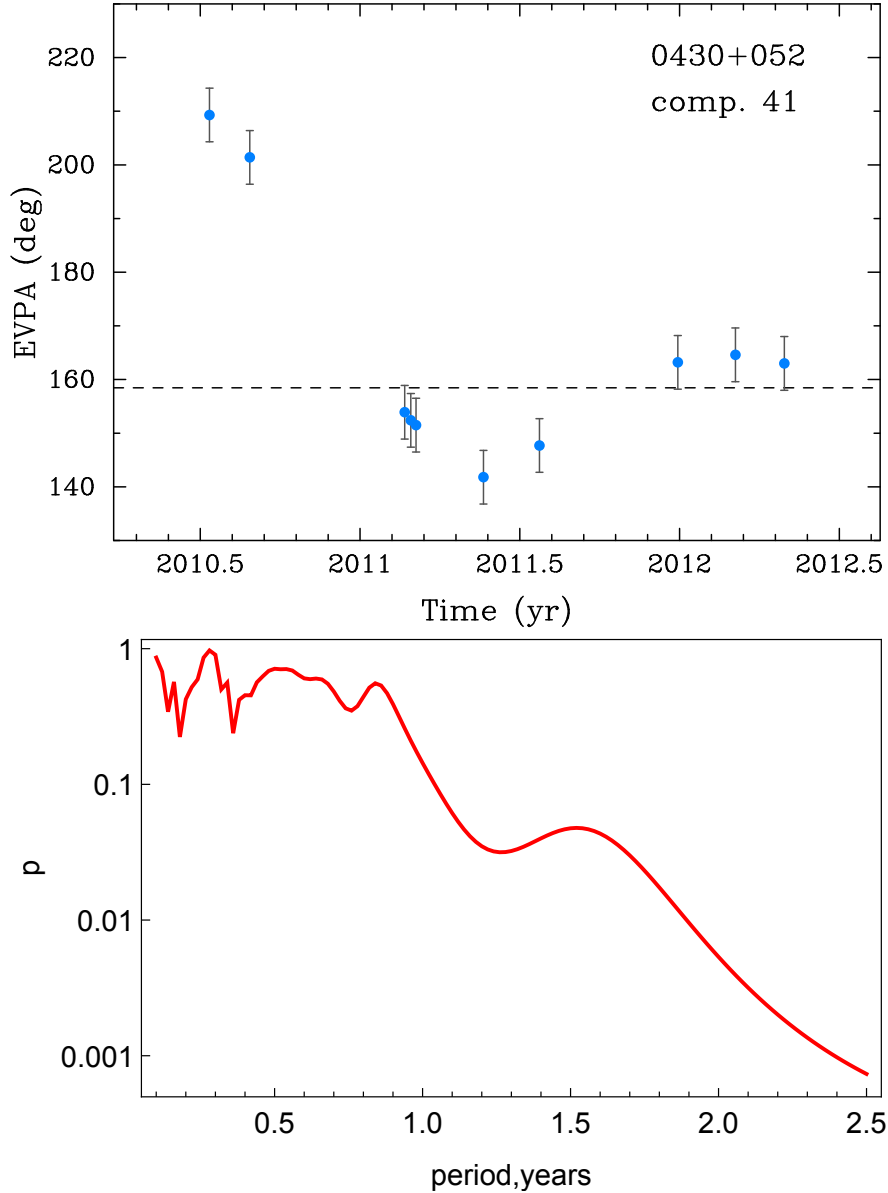


Figure 2. Example of the data and the periodogram for one source component. The EVPA observations of component 41 of 3C 120 are shown versus the observation time (Earth frame, top panel). The p -value calculated from the Lomb–Scargle periodogram for this component is shown as a function of the period T (source frame, i.e. rescaled by $(1+z)$, bottom panel). Low p -values indicate that oscillations with large periods fit the data well; however, they do not affect the resulting significance for the full data set estimated through Monte-Carlo simulations.

of 0.02 yr. This corresponds to the ULDM particle mass $5 \times 10^{-23} \text{ eV} \leq m \leq 1.2 \times 10^{-21} \text{ eV}$, see Section 2. The meaning of the p -value is the probability that a signal of a given power (or stronger) is produced by random Gaussian fluctuations; note that $0 \leq p \leq 1$. In practice, relevant random backgrounds are not distributed normally, and therefore we do not interpret this quantity as a probability. Figure 2 presents an example of the data and the periodogram for one of the source components shown in Figure 1.

Next, we need to consider the ensemble of N time sequences ($N = 32$ in our case). For each time sequence, i.e. for each source component, we have the dependence of the p -value on the period, $p_i(T)$, $i = 1, \dots, N$. For every particular source, small $p_i(T)$ indicates that the data favour, to some extent, oscillations with a period T . Consider now the function

$$L(T) = \log \prod_{i=1}^N p_i(T) = \sum_{i=1}^N \log(p_i(T)).$$

Qualitatively, low $L(T)$ would indicate periodic signals with *the same period* T in different sources, as it is expected in ULDM models. Contrary, if periodicities in individual sources are absent or uncorrelated, as it is expected for their intrinsic origin, minima of $p_i(T)$ would not coincide, and $L(T)$ would not be that low.

What does a particular value of $L(T)$ mean? To understand it in terms of physical quantities, we perform Monte-Carlo simulations of many artificial data sets, both without the ULDM effect and with the EVPA oscillations with the common period and amplitude introduced by hand, for various periods and amplitudes. The simulations are described in detail in Appendix B. The simulations of random sets, Section B.1, allow one to answer the question how often a given value of $L(T)$ may be obtained as a random fluctuation of the data with no signal for a given T , thus attributing a local p -value to the observed realization of $L(T)$ for the ensemble of sources. The global significance of the observed deviation from randomness is estimated through the same simulation as a measure of the fraction of MC sets for which this or lower p -value is obtained from fluctuations for *any* T .

To convert $L(T)$ into a limit on the amplitude of EVPA oscillations ϕ , we use the simulations described in Section B.2, when signals with various ϕ are artificially added to the random data. From these simulations we determine for which ϕ a given or lower value of $L(T)$ occurs in 95% of simulated data sets. This allows us to derive the 95% CL upper limit on ϕ for every T . These upper limits on the common amplitude ϕ at a given common period T are finally translated into the limits on the axion-photon coupling $g_{a\gamma}$ at a given ALP mass m using Eqs. (2.1), (2.2) derived in Section 2.

5 Results and discussion

We turn now to the results of the data analysis. They are presented in Figures 3, 4, 5, 6.

Figure 3 presents values of L for various oscillation periods T , as expected from MC simulations (for the case of no ULDM effect) and observed in real data. The observed $L(T)$ is in good agreement with expectations, indicating that no ULDM effect is seen. Figure 4 confirms this by presenting p -values which correspond to probabilities of obtaining the observed or lower $L(T)$ in Monte-Carlo simulated sets: the local p -value corresponds to a given T while the global p -value is the probability to observe this or lower local p -value for any T . The corresponding 95% CL upper limits on the amplitude $\phi(T)$ are given in Figure 5. They are interpreted in terms of physical parameters of ALP in Figure 6. Note that the conversion of the limits on the EVPA oscillation amplitude versus T into the limits on $g_{a\gamma}(m)$, that is the transition from Figure 5 to Figure 6, is subject to theoretical systematic uncertainties, the main of which is the lack of knowledge of the dark-matter density in particular observed sources, encoded in the parameter $\kappa \equiv \rho_{\text{DM}}/(20 \text{ GeV}/\text{cm}^3)$. Our limits on $g_{a\gamma}$ scale with $\kappa^{1/2}$.

We turn now to the comparison of our results with other available constraints on $g_{a\gamma}$ for ULDM ALPs. One should note here that the scalar ULDM with masses below $\sim 10^{-21}$ eV

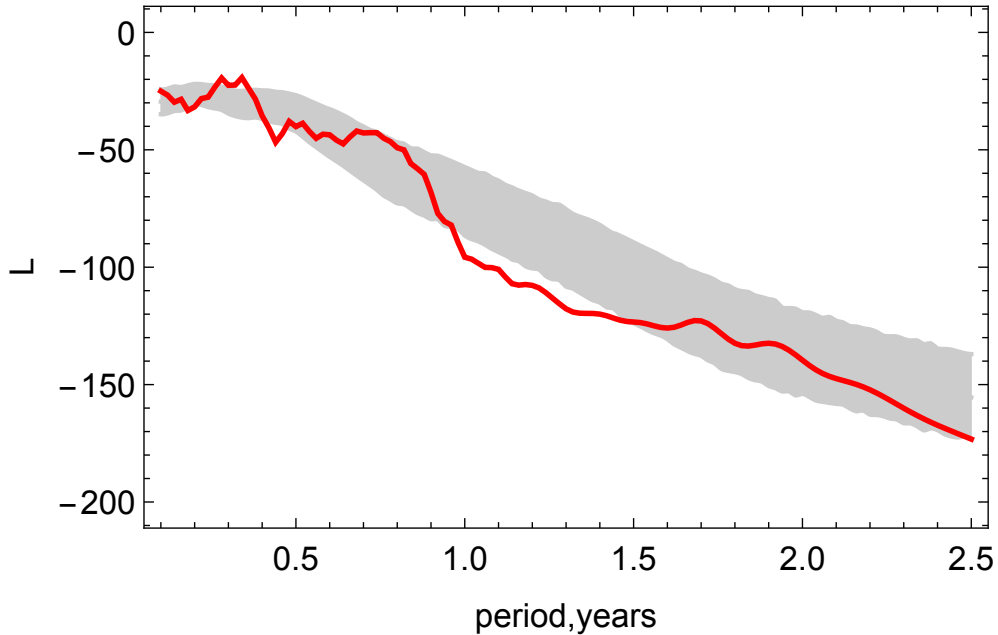


Figure 3. Expected in the case of no ULDM effect (gray band, 68% CL) and observed (thick red line) L as a function of the period T .

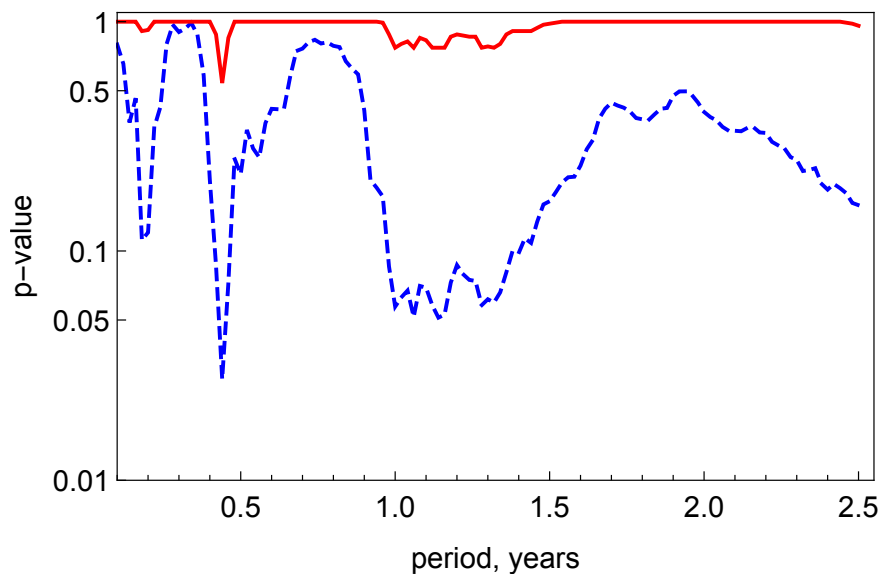


Figure 4. Local (dashed blue line) and global (full red line) p-values for deviations of the observed value of L from the expected one, as a function of the period T .

is disfavoured by the Lyman-alpha forest measurements [58]. However, these constraints are not applicable for certain models with ULDM ALPs, see e.g. Ref. [59].

The most abundant group of constraints includes those based on astrophysical effects of ALPs independent on whether they form the dark matter or not. The least model dependent bound results from non-observation of ALPs coming from the Sun with a dedicated axion helioscope, CAST [60]. A quantitatively similar constraint comes from the analysis

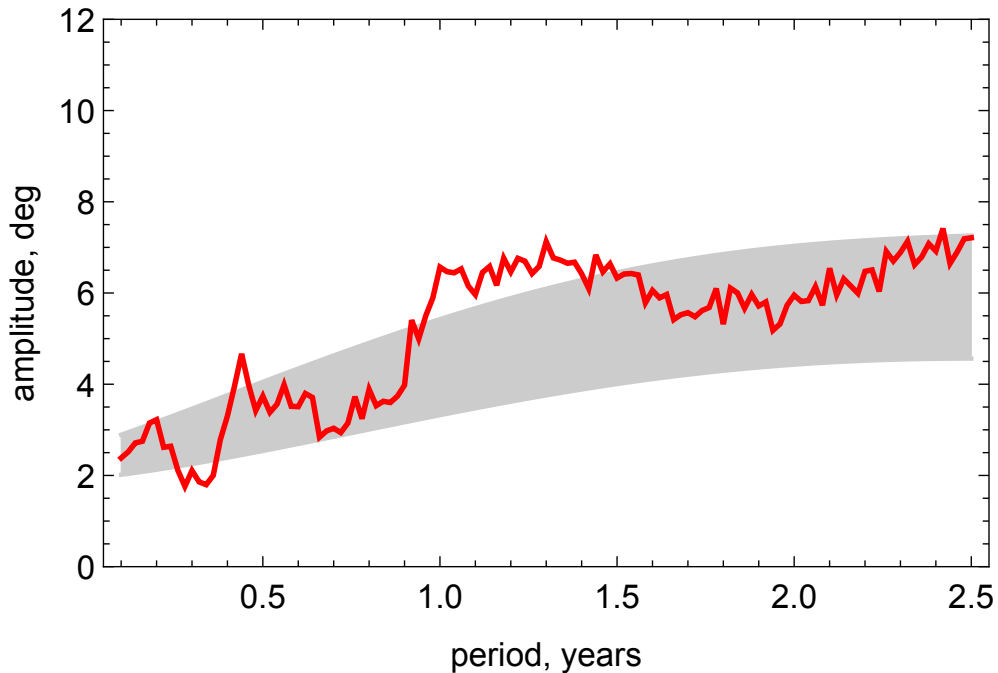


Figure 5. Expected in the case of no ULDM effect (gray band, 68% CL) and observed (thick red line) 95% CL upper limits on the amplitude of oscillations ϕ as a function of the period T .

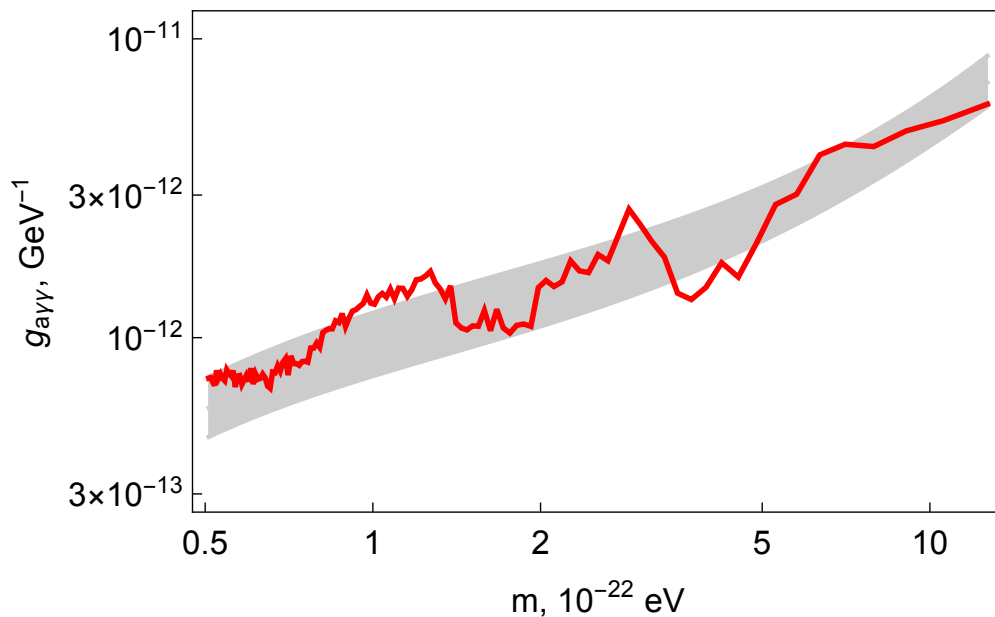


Figure 6. Expected in the case of no ULDM effect (gray band, 68% CL) and observed (thick red line) 95% CL upper limits on the axion-photon coupling $g_{a\gamma}$ as a function of the ALP mass m , for $\kappa = 1$.

of energy losses in horizontal-branch stars in globular clusters [61]. A stronger, but more model dependent constraint was derived from non-observation of gamma rays from supernova SN 1987A [62]. A series of constraints have been obtained from the absence of spectral

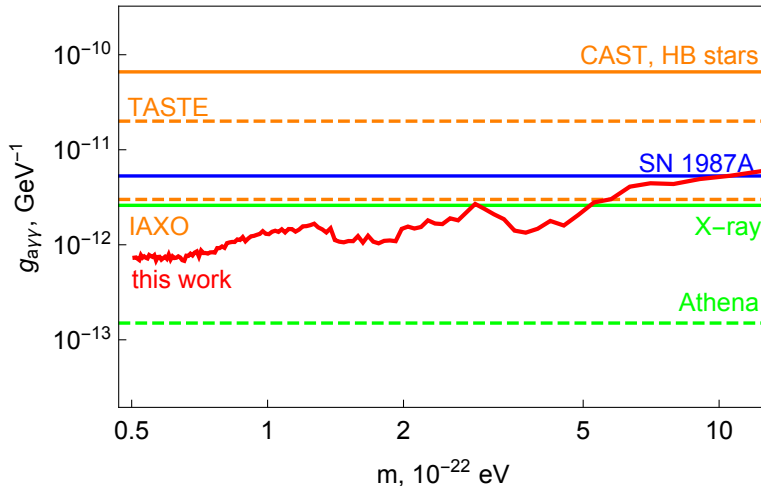


Figure 7. Upper limits on the axion-photon coupling $g_{a\gamma}$ as a function of the ALP mass m from astrophysical effects (not necessary assuming ULDM): solar axion searches with CAST [60], energy losses of the horizontal-branch (HB) stars [61] (quantitatively the same as CAST), absence of gamma rays from SN 1987A [62] and absence of spectral irregularities in the X-ray spectrum of Vir A [65] (see the text for more references and discussions of caveats). Projected sensitivities of axion helioscopes TASTE [67] and IAXO [68], as well as of the search for X-ray spectral irregularities with Athena [69] are shown by dashed lines. The limit from the present work ($\kappa = 1$) is given by the full red line for comparison.

irregularities of X-ray sources embedded in the galaxy clusters, see Refs. [63–66]. These constraints are heavily based on the modelling of the magnetic fields in the clusters which is far from being certain. One of the strongest constraints comes from the nearby Virgo cluster [65] for which the turbulent component of the magnetic field was modelled with a certain level of confidence². In all these studies, a possible regular component of the cluster magnetic field was ignored, which makes the conclusions less robust. The astrophysical constraints are compared to our results in Figure 7, where we also show projected sensitivities of helioscope experiments TASTE [67] and IAXO [68], as well as the expected sensitivity of X-ray irregularity analysis with the future instrument Athena [69].

Perfectly model-independent results come from purely laboratory experiments, which include “light shining through walls” (e.g. ALPS-I [70] and OSQAR [71]) and searches for vacuum birefringence, PVLAS [72]. Though this approach is the most robust, it results in constraints on ALPs several orders of magnitude worse than astrophysical ones, just because of limitations of the terrestrial equipment as compared to astrophysical environments. The laboratory constraints, as well as the ones expected from the resonant-regeneration ALPS-IIc experiment [73], are compared to our results in Figure 8.

6 Conclusions

Certain dark-matter models assume that ultra-light axion-like particles form a condensate, coherently oscillating with a period of about a year in domains of about 100 pc. These oscillations get imprinted on the polarization angle of linearly polarized electromagnetic emission

²A slightly stronger constraint was reported in Ref. [66] for a Seyfert galaxy 2E 3140 in the Abell 1795 cluster; however, the precise location of this galaxy within the cluster is unknown.

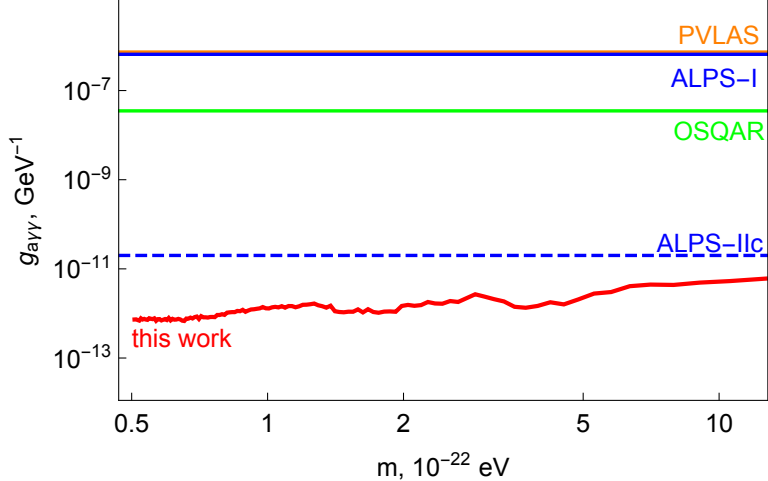


Figure 8. Upper limits on the axion-photon coupling $g_{a\gamma}$ as a function of the ALP mass m from purely laboratory searches: ALPS-I [70], PVLAS [72] and OSQAR [71]. Projected sensitivity of ALPS-IIc [73] is shown by the dashed line. The limit from the present work ($\kappa = 1$) is given by the full red line for comparison.

of astrophysical sources. The period of the oscillations in the source frame is universal and is determined by the particle mass only, so that the corresponding periodic changes would be present for various sources with the same period.

In the present work, we used the data obtained in long-term polarization measurements of parsec-scale jets in active galactic nuclei within the MOJAVE project to search for such periodic patterns with a common period. We did not find any statistically significant effect and have obtained constraints on the photon coupling to axion-like ultralight dark matter at the level of $\lesssim 10^{-12} \text{ GeV}^{-1}$ for masses between $\sim 5 \times 10^{-23} \text{ eV}$ and $\sim 1.2 \times 10^{-21} \text{ eV}$.

Acknowledgments

We are indebted to Grigory Rubtsov, Sergey Sibiryakov, Guenter Sigl and Peter Tinyakov for interesting and helpful discussions and to Eduardo Ros for useful comments on the manuscript. This research has made use of data from the MOJAVE data base, which is maintained by the MOJAVE team [46]. The MOJAVE project was supported by NASA-*Fermi* GI grants NNX08AV67G, NNX12A087G, and NNX15AU76G. Y.K. and A.B.P. are partly supported by the Russian Foundation for Basic Research (project 17-02-00197) and the government of the Russian Federation (agreement 05.Y09.21.0018). T.S. was funded by the Academy of Finland projects 274477, 284495 and 312496. The work of M.I. and S.T. on constraining parameters of ultra-light axions with astrophysical methods is supported by the Russian Science Foundation (grant 18-12-00258). S.T. thanks CERN Theory Department for hospitality at the final stages of this work.

Note added. When this study was finalized, two preprints have been posted on arXiv which study constraints on $g_{a\gamma}$ for ULDM ALPs within different approaches. Like our study, they are based on polarization effects, but do not consider the periodic oscillations which are at the base of our method. They include the search for birefringence in observations of the protoplanetary disk of AB Aur [74] and the Cosmic Microwave Background [75] at the cosmological and

Galactic scales. They report upper limits of $g_{a\gamma} \lesssim 10^{-13} \text{ GeV}^{-1}$ for $m \sim 10^{-22} \text{ eV}$. While a detailed discussion of these results is beyond the scope of the present paper, we note that both Refs. [74] and [75] assume an additional enhancement of the polarization-angle rotation by a factor of \sqrt{n} , where n is the number of $\sim 100 \text{ pc}$ ALP-field domains crossed by the light on its way from the source to the observer. This enhancement is at odds with earlier works [19, 29] (in more detail, corrections to the results of Ref. [29] will be discussed elsewhere [76]). This \sqrt{n} factor is close to one for AB Aur, which is only 163 pc away; however, the observations [77] used in Ref. [74] continued only for $\sim 3 \text{ min}$ and therefore give only a snapshot of possible EVPA oscillations. Observations of this kind would be a very prospective tool to constrain $g_{a\gamma}$ if they were performed at several epochs and for several sources, like those used in the present paper.

A Generalized Lomb–Scargle periodogram

In this Appendix, we collect, for convenience, the formulae used to derive the generalized Lomb–Scargle periodogram, following Ref. [55].

Consider a series of N measurements of a quantity $y_i \pm \sigma_i$, performed at epochs t_i , $i = 1, \dots, N$. Introduce vectors of the time arguments $\mathbf{t} = \{t_i\}$, data values $\mathbf{y} = \{y_i\}$ and inverse errors $\bar{\boldsymbol{\sigma}} = \{1/\sigma_i\}$. Determine the vector of normalized weights $\mathbf{w} = \{w_i\}$ with

$$w_i = \frac{1}{\bar{\boldsymbol{\sigma}} \cdot \bar{\boldsymbol{\sigma}}} \frac{1}{\sigma_i^2},$$

satisfying $\sum w_i = 1$ (hereafter the vectors are denoted by bold face, the dot between two vectors denotes their scalar product while the dot between two scalars denotes their product).

For every period T we want to consider, denote $\mathbf{C} = \{\cos(\omega t_i)\}$ and $\mathbf{S} = \{\sin(\omega t_i)\}$, where $\omega = 2\pi/T$. One further denotes:

$$\begin{aligned} Y &= \mathbf{w} \cdot \mathbf{y}, & C &= \mathbf{w} \cdot \mathbf{C}, & S &= \mathbf{w} \cdot \mathbf{S}, \\ \hat{Y}_Y &= \sum w_i y_i^2, & Y_Y &= \hat{Y}_Y - Y \cdot Y, \\ \hat{Y}_C &= \sum w_i y_i c_i, & Y_C &= \hat{Y}_C - Y \cdot C, \\ \hat{Y}_S &= \sum w_i y_i s_i, & Y_S &= \hat{Y}_S - Y \cdot S, \\ \hat{C}_C &= \sum w_i c_i^2, & C_C &= \hat{C}_C - C \cdot C, \\ \hat{S}_S &= 1 - \hat{C}_C, & S_S &= \hat{S}_S - S \cdot S, \\ \hat{C}_S &= \sum w_i c_i s_i, & C_S &= \hat{C}_S - C \cdot S, \\ D &= C_C \cdot S_S - C_S \cdot C_S. \end{aligned}$$

The power spectrum (“normalized periodogram”) is then determined as

$$P(\omega) = \frac{1}{Y_Y \cdot D} (S_S \cdot Y_C \cdot Y_C + C_C \cdot Y_S \cdot Y_S - 2C_S \cdot Y_C \cdot Y_S).$$

One notes that $0 \leq P(\omega) \leq 1$. The local p -value for a given frequency ω is

$$p(\omega) = (1 - P(\omega))^{\frac{N-3}{2}}.$$

To obtain the global significance of a minimum in $p(\omega)$, one needs a more complicated account of the look-elsewhere correction, which may be achieved, for instance, by the Monte-Carlo simulations.

B Monte-Carlo simulations and expected limits

B.1 Monte-Carlo simulation

To perform statistical studies of the data used in this work, we need to compare actual results with those expected for random data sets, in generation of which one assumes the absence of the effect we are looking for. Generation of these sets is not straightforward because the actual data may have intrinsic non-randomness not related to the effect of ULDM. In particular, intrinsic conditions in the sources may induce periodic or quasi-periodic oscillations of EVPA, see e.g. Refs. [78, 79]: we do not know in advance whether these features are present or not. Therefore, assuming fully random values of EVPA based on the experimental error bars would be misleading: to imitate the ULDM effect in such MC sets, (i) periodic fluctuations should appear in various sources and (ii) their periods, by chance, should coincide. If, however, intrinsic periodic background is present in particular sources, the true probability to initiate the signal from fluctuations is determined by (ii) only. We therefore need to keep unknown features, including periodic ones, in the simulated data sets.

To this end, we adopt a time-scaling procedure: to generate MC time series of EVPA measurements for a source, we take the actual data (t_i, y_i) and introduce the factor ξ , a random number uniformly distributed between 0.5 and 2.5, by which the observational time is scaled. The simulated data set is then (t'_i, y_i) , where

$$t'_i = t_1 + \xi(t_i - t_1)$$

(the measured values of EVPA, y_i , are taken from the actual data set). The value of ξ is chosen randomly for every source in the sample. In this way, any potential ULDM signal (periodic changes with a common period for all sources in the set), which might be present in the data, is removed while any intrinsic features, including individual periodicity, remain.

B.2 Estimate of the expected limits

To estimate the limits on the amplitude ϕ of periodic oscillations of the polarization angle, we use the following procedure. We generate a large number (2500 for each value of the period T considered) of MC data sets assuming no common periodic effects are present beyond those generated randomly. For every artificial data set, we reconstruct and record the value of L , as described in Sec. 4, as a function of T . For each given T , we determine the 68% CL band, $\Delta L_{68}(T)$, and the mean, $L_{\text{mean}}(T)$, of the values of L which assume no signal (see Figure 9, upper panel). This is the band presented in Figure 3 of the main text together with the function $L(T)$ obtained for the real data.

Next, we perform another MC simulation, this time assuming that some ULDM effect is present. For each fixed period T , we generate 2500 MC data sets as described above, but with artificially added harmonic oscillations with period T , amplitude ϕ (fixed for all objects in the set but random from one MC set to another, following a uniform distribution between 0° and 15°) and phases δ_i (random for every object in every MC set). Then, still for the fixed T , we determine the 95% upper limit on ϕ as a function of L as follows. Take the interval $(L - \epsilon, L + \epsilon)$ for a sufficiently small ϵ ($\epsilon = 5$ was used) to have enough data points in this interval and find the value ϕ_{95} such that 95% of the MC points in the interval have $\phi < \phi_{95}$. This, for each given T , allows us to obtain the function $\phi_{95}(L)$ which we fit by a smooth 4-parametric curve to suppress fluctuations related to particular MC realizations. This function is presented in Figure 9 (lower panel) as a thick red curve for a particular value

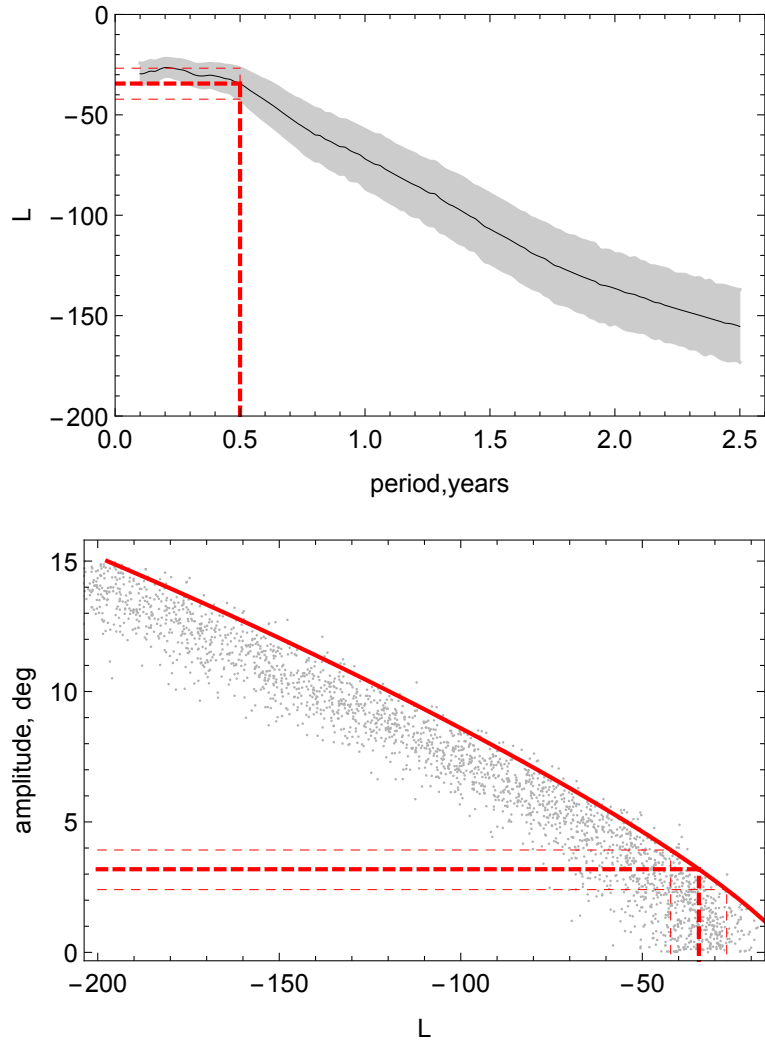


Figure 9. Calculation of the expected limit based on MC simulations. The upper panel presents the scatter of $L(T)$ in random MC samples (the full line is the mean value and the gray band contains 68% of MC points for a given T). For example, for $T = 0.5$ yr, the mean value and the 68% band are shown by thick and thin dashed red lines, respectively. The lower panel is based on the Monte-Carlo samples with artificially introduced periodic oscillations of EVPA with a period of 0.5 years and various amplitudes and phases. For a given value of L , 95% of the points are below the full red line. The determination of the mean expected 95% CL upper limit and its 68% CL expected range, based on the values of L obtained from the upper panel, is shown by dashed lines.

of $T = 0.5$ yr. The values of $\phi_{95}(L_{\text{mean}})$ and $\phi_{95}(\Delta L_{68})$, with the values of the arguments obtained at the previous step, give the mean value and the 68% CL band for the expected 95% CL upper limit on ϕ for a given T , assuming that no ULDM effect is present. This results in the band of expected upper limits as a function of T , presented in Figure 5 of the main text together with the limits obtained from the real data in the same way.

References

- [1] T. Marrodan Undagoitia and L. Rauch, *Dark matter direct-detection experiments*, *J. Phys. G* **43** (2016) 013001 [arXiv:1509.08767 [physics.ins-det]].
- [2] A. Boveia and C. Doglioni, *Dark Matter Searches at Colliders*, *Ann. Rev. Nucl. Part. Sci.* **68** (2018) 429 [arXiv:1810.12238 [hep-ex]].
- [3] J. Conrad, J. Cohen-Tanugi and L. E. Strigari, *WIMP searches with gamma rays in the Fermi era: challenges, methods and results*, *J. Exp. Theor. Phys.* **121** (2015) 1104 [*Zh. Eksp. Teor. Fiz.* **148** (2015) no.6, 1257] [arXiv:1503.06348 [astro-ph.CO]].
- [4] D. H. Weinberg *et al.*, *Cold dark matter: controversies on small scales*, *Proc. Nat. Acad. Sci.* **112** (2015) 12249 [arXiv:1306.0913 [astro-ph.CO]].
- [5] A. A. Klypin *et al.*, *Where are the missing Galactic satellites?*, *Astrophys. J.* **522** (1999) 82 [astro-ph/9901240].
- [6] B. Moore *et al.*, *Dark matter substructure within galactic halos*, *Astrophys. J.* **524** (1999) L19 [astro-ph/9907411].
- [7] M. Boylan-Kolchin, J. S. Bullock and M. Kaplinghat, *Too big to fail? The puzzling darkness of massive Milky Way subhaloes*, *Mon. Not. Roy. Astron. Soc.* **415** (2011) L40 [arXiv:1103.0007 [astro-ph.CO]].
- [8] R. F. G. Wyse and G. Gilmore, *Observed Properties of Dark Matter on Small Spatial Scales*, *IAU Symp.* **244** (2008) 44 [arXiv:0708.1492 [astro-ph]].
- [9] P. J. E. Peebles, *Fluid dark matter*, *Astrophys. J.* **534** (2000) L127 [astro-ph/0002495].
- [10] J. Goodman, *Repulsive dark matter*, *New Astron.* **5** (2000) 103 [astro-ph/0003018].
- [11] W. Hu, R. Barkana and A. Gruzinov, *Cold and fuzzy dark matter*, *Phys. Rev. Lett.* **85** (2000) 1158 [astro-ph/0003365].
- [12] M. S. Turner, *Coherent Scalar Field Oscillations in an Expanding Universe*, *Phys. Rev. D* **28** (1983) 1243.
- [13] I. I. Tkachev, *Coherent Scalar-Field Oscillations Forming Compact Astrophysical Object*, *Sov. Astron. Lett.* **12** (1986) 305 [*Pisma v Astron. Zh.* **12** (1986) 726].
- [14] M. Khlopov, B. A. Malomed and I. B. Zeldovich, *Gravitational instability of scalar fields and formation of primordial black holes*, *Mon. Not. Roy. Astron. Soc.* **215** (1985) 575.
- [15] D. J. E. Marsh, *Axion Cosmology*, *Phys. Rept.* **643** (2016) 1 [arXiv:1510.07633 [astro-ph.CO]].
- [16] L. Hui *et al.*, *Ultralight scalars as cosmological dark matter*, *Phys. Rev. D* **95** (2017) 043541 [arXiv:1610.08297 [astro-ph.CO]].
- [17] J. Jaeckel and A. Ringwald, *The Low-Energy Frontier of Particle Physics*, *Ann. Rev. Nucl. Part. Sci.* **60** (2010) 405 [arXiv:1002.0329 [hep-ph]].
- [18] P. Svrcek and E. Witten, *Axions In String Theory*, *JHEP* **0606** (2006) 051 [hep-th/0605206].
- [19] A. Arvanitaki *et al.*, *String Axiverse*, *Phys. Rev. D* **81** (2010) 123530 [arXiv:0905.4720 [hep-th]].
- [20] M. Cicoli, M. Goodsell and A. Ringwald, *The type IIB string axiverse and its low-energy phenomenology*, *JHEP* **1210** (2012) 146 [arXiv:1206.0819 [hep-th]].
- [21] I. G. Irastorza and J. Redondo, *New experimental approaches in the search for axion-like particles*, *Prog. Part. Nucl. Phys.* **102** (2018) 89 [arXiv:1801.08127 [hep-ph]].
- [22] M. Giannotti *et al.*, *Stellar Recipes for Axion Hunters*, *JCAP* **1710** (2017) 010 [arXiv:1708.02111 [hep-ph]].
- [23] S. V. Troitsky, *Axion-like particles and the propagation of gamma rays over astronomical distances*, *JETP Lett.* **105** (2017) 55 [arXiv:1612.01864 [astro-ph.HE]].

- [24] G. Raffelt and L. Stodolsky, *Mixing of the Photon with Low Mass Particles*, *Phys. Rev. D* **37** (1988) 1237.
- [25] H. Y. Schive, T. Chiueh and T. Broadhurst, *Cosmic Structure as the Quantum Interference of a Coherent Dark Wave*, *Nature Phys.* **10** (2014) 496 [arXiv:1406.6586 [astro-ph.GA]].
- [26] A. Khmelnitsky and V. Rubakov, *Pulsar timing signal from ultralight scalar dark matter*, *JCAP* **1402** (2014) 019 [arXiv:1309.5888 [astro-ph.CO]].
- [27] N. K. Porayko and K. A. Postnov, *Constraints on ultralight scalar dark matter from pulsar timing*, *Phys. Rev. D* **90** (2014) 062008 [arXiv:1408.4670 [astro-ph.CO]].
- [28] N. K. Porayko *et al.*, *Parkes Pulsar Timing Array constraints on ultralight scalar-field dark matter*, *Phys. Rev. D* **98** (2018) 102002 [arXiv:1810.03227 [astro-ph.CO]].
- [29] D. Harari and P. Sikivie, *Effects of a Nambu-Goldstone boson on the polarization of radio galaxies and the cosmic microwave background*, *Phys. Lett. B* **289**, 67 (1992).
- [30] J. F. C. Wardle, R. A. Perley and M. H. Cohen, *Observational evidence against birefringence over cosmological distances*, *Phys. Rev. Lett.* **79** (1997) 1801 [astro-ph/9705142].
- [31] F. Finelli and M. Galaverni, *Rotation of Linear Polarization Plane and Circular Polarization from Cosmological Pseudo-Scalar Fields*, *Phys. Rev. D* **79**, 063002 (2009) [arXiv:0802.4210 [astro-ph]].
- [32] S. di Serego Alighieri, F. Finelli and M. Galaverni, *Limits on Cosmological Birefringence from the UV Polarization of Distant Radio Galaxies*, *Astrophys. J.* **715**, 33 (2010) [arXiv:1003.4823 [astro-ph.CO]].
- [33] M. Galaverni *et al.*, *Cosmological birefringence constraints from CMB and astrophysical polarization data*, *JCAP* **1508**, no. 08, 031 (2015) [arXiv:1411.6287 [astro-ph.CO]].
- [34] I. Obata, T. Fujita and Y. Michimura, *Optical Ring Cavity Search for Axion Dark Matter*, *Phys. Rev. Lett.* **121**, 161301 (2018) [arXiv:1805.11753 [astro-ph.CO]].
- [35] W. DeRocco and A. Hook, *Axion interferometry*, *Phys. Rev. D* **98** 035021 (2018) [arXiv:1802.07273 [hep-ph]].
- [36] H. Liu *et al.*, *Searching for Axion Dark Matter with Birefringent Cavities*, arXiv:1809.01656 [hep-ph].
- [37] N. Lyskova, E. Churazov, T. Naab, *Mass density slope of elliptical galaxies from strong lensing and resolved stellar kinematics* *Mon. Not. Roy. Astron. Soc.* **475**, 2403 (2018) [1711.01123 [astro-ph.GA]].
- [38] N. Lyskova *et al.*, *Stellar kinematics of X-ray bright massive elliptical galaxies*, *Mon. Not. Roy. Astron. Soc.* **441** (2014) 2013 [arXiv:1404.2729 [astro-ph.GA]].
- [39] E.W. Greisen, *AIPS, the VLA, and the VLBA*, in: *Astrophysics and Space Science Library 285, Information Handling in Astronomy – Historical Vistas*, Ed. A. Heck, Dordrecht: Kluwer (2003) 109
- [40] M.C. Shepherd, *Difmap: an Interactive Program for Synthesis Imaging*, in: *Astronomical Data Analysis Software and Systems VI*, Eds. G. Hunt and H.E. Payne, San Francisco: ASP, Astronomical Society of the Pacific Conference Series, **125** (1997) 77.
- [41] M. L. Lister *et al.*, *MOJAVE: Monitoring of Jets in AGN with VLBA Experiments. V. Multi-epoch VLBA Images*, *Astron. J.* **137** (2009) 3718 [arXiv:0812.3947 [astro-ph]].
- [42] M. L. Lister *et al.*, *MOJAVE XIII. Parsec-Scale AGN Jet Kinematics Analysis Based on 19 years of VLBA Observations at 15 GHz*, *Astron. J.* **152** (2016) 12 [arXiv:1603.03882 [astro-ph.GA]].
- [43] D. C. Homan *et al.*, *MOJAVE XII: Acceleration and Collimation of Blazar Jets on Parsec Scales*, *Astrophys. J.* **798** (2015) 134 [arXiv:1410.8502 [astro-ph.HE]].

- [44] D. C. Homan and M. L. Lister, *MOJAVE: Monitoring of Jets in Active Galactice Nuclei with VLBA Experiments. II. First-Epoch 15-GHz Circular Polarization Results*, *Astron. J.* **131** (2006) 1262 [astro-ph/0511838].
- [45] M. L. Lister and D. C. Homan, *MOJAVE: Monitoring of jets in AGN with VLBA experiments. I. First-epoch 15-GHz linear polarization images*, *Astron. J.* **130** (2005) 1389 [astro-ph/0503152].
- [46] M.L. Lister *et al.*, *MOJAVE. XV. VLBA 15 GHz Total Intensity and Polarization Maps of 437 Parsec-scale AGN Jets from 1996 to 2017*, *Astrophys. J. Suppl.* **234** (2018) 12 [arXiv:1711.07802 [astro-ph.GA]].
- [47] M.A. Hodge *et al.*, *MOJAVE XVI: Multiepoch Linear Polarization Properties of Parsec-scale AGN Jet Cores*, *Astrophys. J.* **862** (2018) 151 [arXiv:1806.07312 [astro-ph.GA]].
- [48] A. Pushkarev *et al.*, *Linear Polarization Properties of Parsec-Scale AGN Jets, Galaxies* **5** (2017) 93 [arXiv:1712.03025 [astro-ph.GA]].
- [49] M.L. Lister *et al.*, in preparation.
- [50] A.V. Plavin *et al.*, *Significant core shift variability in parsec-scale jets of active galactic nuclei*, *MNRAS*, submitted (2018) [arXiv:1811.02544 [astro-ph.GA]].
- [51] A. P. Marscher, *Turbulent, Extreme Multi-zone Model for Simulating Flux and Polarization Variability in Blazars*, *Astrophys. J.* **780** (2014) 87 [arXiv:1311.7665 [astro-ph.HE]].
- [52] J.F.C. Wardle and P.P. Kronberg, *The linear polarization of quasi-stellar radio sources at 3.71 and 11.1 centimeters*, *Astrophys. J.* **194** (1974) 249.
- [53] A.R. Taylor *et al.*, *A Rotation Measure Image of the Sky*, *Astrophys. J.* **702** (2009) 1230.
- [54] N. Oppermann *et al.*, *An improved map of the Galactic Faraday sky*, *Astron. Astrophys.* **542** (2012) A93 [arXiv:1111.6186 [astro-ph.GA]].
- [55] M. Zechmeister and M. Kurster, *The generalised Lomb-Scargle periodogram. A new formalism for the floating-mean and Keplerian periodograms*, *Astron. Astrophys.* **496** (2009) 577 [arXiv:0901.2573 [astro-ph.IM]].
- [56] J. T. VanderPlas, *Understanding the Lomb-Scargle Periodogram*, *Astrophys. J. Suppl.* **236** (2018) 16 [arXiv:1703.09824 [astro-ph.IM]].
- [57] P. Gregory, *Bayesian Logical Data Analysis for the Physical Sciences*, Cambridge Univ. Press, 2010
- [58] V. Irsic *et al.*, *First constraints on fuzzy dark matter from Lyman- α forest data and hydrodynamical simulations*, *Phys. Rev. Lett.* **119** (2017) 031302 [arXiv:1703.04683 [astro-ph.CO]].
- [59] K. H. Leong, H. Y. Schive, U. H. Zhang and T. Chiueh, *Testing extreme-axion wave dark matter using the BOSS Lyman-Alpha forest data*, arXiv:1810.05930 [astro-ph.CO].
- [60] V. Anastassopoulos *et al.* [CAST Collaboration], *New CAST Limit on the Axion-Photon Interaction*, *Nature Phys.* **13** (2017) 584 [arXiv:1705.02290 [hep-ex]].
- [61] A. Ayala *et al.*, *Revisiting the bound on axion-photon coupling from Globular Clusters*, *Phys. Rev. Lett.* **113** (2014) no.19, 191302 [arXiv:1406.6053 [astro-ph.SR]].
- [62] A. Payez *et al.*, *Revisiting the SN1987A gamma-ray limit on ultralight axion-like particles*, *JCAP* **1502** (2015) 006 [arXiv:1410.3747 [astro-ph.HE]].
- [63] D. Wouters and P. Brun, *Constraints on Axion-like Particles from X-Ray Observations of the Hydra Galaxy Cluster*, *Astrophys. J.* **772** (2013) 44 [arXiv:1304.0989 [astro-ph.HE]].
- [64] M. Berg *et al.*, *Constraints on Axion-Like Particles from X-ray Observations of NGC 1275*, *Astrophys. J.* **847** (2017) 101 [arXiv:1605.01043 [astro-ph.HE]].

- [65] M. C. D. Marsh *et al.*, *A New Bound on Axion-Like Particles*, *JCAP* **1712** (2017) 036 [arXiv:1703.07354 [hep-ph]].
- [66] J. P. Conlon *et al.*, *Constraints on Axion-Like Particles from Non-Observation of Spectral Modulations for X-ray Point Sources*, *JCAP* **1707** (2017) 005 [arXiv:1704.05256 [astro-ph.HE]].
- [67] V. Anastassopoulos *et al.* [TASTE Collaboration], *Towards a medium-scale axion helioscope and haloscope*, *JINST* **12** (2017) no.11, P11019 [arXiv:1706.09378 [hep-ph]].
- [68] I. G. Irastorza *et al.*, *Towards a new generation axion helioscope*, *JCAP* **1106** (2011) 013 [arXiv:1103.5334 [hep-ex]].
- [69] J. P. Conlon, F. Day, N. Jennings, S. Krippendorf and F. Muia, *Projected bounds on ALPs from Athena*, *Mon. Not. Roy. Astron. Soc.* **473** (2018) 4932 [arXiv:1707.00176 [astro-ph.HE]].
- [70] K. Ehret *et al.*, *New ALPS Results on Hidden-Sector Lightweights*, *Phys. Lett. B* **689** (2010) 149 [arXiv:1004.1313 [hep-ex]].
- [71] R. Ballou *et al.* [OSQAR Collaboration], *New exclusion limits on scalar and pseudoscalar axionlike particles from light shining through a wall*, *Phys. Rev. D* **92** (2015) 092002 [arXiv:1506.08082 [hep-ex]].
- [72] F. Della Valle *et al.*, *The PVLAS experiment: measuring vacuum magnetic birefringence and dichroism with a birefringent Fabry-Perot cavity*, *Eur. Phys. J. C* **76** (2016) 24 [arXiv:1510.08052 [physics.optics]].
- [73] R. Bahre *et al.*, *Any light particle search II -Technical Design Report*, *JINST* **8** (2013) T09001 [arXiv:1302.5647 [physics.ins-det]].
- [74] T. Fujita, R. Tazaki and K. Toma, *Hunting Axion Dark Matter with Protoplanetary Disks*, arXiv:1811.03525 [astro-ph.CO].
- [75] G. Sigl, P. Trivedi, *Axion-like Dark Matter Constraints from CMB Birefringence*, arXiv:1811.07873 [astro-ph.CO].
- [76] M. Ivanov and A. Panin, in preparation.
- [77] J. Hashimoto *et al.*, *Direct Imaging of Fine Structures in Giant Planet Forming Regions of the Protoplanetary Disk around AB Aurigae*, *Astrophys. J.* **729** (2011) [arXiv:1102.4408 [astro-ph.SR]].
- [78] M. H. Cohen *et al.*, *Reversals in the Direction of Polarization Rotation in OJ 287*, *Astrophys. J.* **862** (2018) 1 [arXiv:1806.02870 [astro-ph.GA]].
- [79] H. Zhang *et al.*, *Large-Amplitude Blazar Polarization Angle Swing as a Signature of Magnetic Reconnection*, *Astrophys. J.* **862** (2018) L25 [arXiv:1807.08420 [astro-ph.HE]].